UC Riverside
2017 Publications

Title

Hydroxyl radical formation and soluble trace metal content in particulate matter from renewable diesel and ultra low sulfur diesel in at-sea operations of a research vessel

Permalink

https://escholarship.org/uc/item/85s841jj

Journal

Aerosol Science and Technology, 51(2)

ISSN

0278-6826 1521-7388

Authors

Kuang, Xiaobi M
Scott, John A
da Rocha, Gisele O
et al.

Publication Date

2017-01-13

DOI

10.1080/02786826.2016.1271938

Peer reviewed

Hydroxyl radical formation and soluble trace metal content in particulate matter from renewable diesel and ultra low sulfur diesel in at-sea operations of a research vessel

Xiaobi M. Kuang, John A. Scott, Gisele O. da Rocha, Raghu Betha, Derek J. Price, Lynn M. Russell, David R. Cocker & Suzanne E. Paulson

Taylor & Francis
Taylor & Francis Group
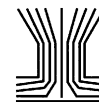
Hydroxyl radical formation and soluble trace metal content in particulate matter from renewable diesel and ultra low sulfur diesel in at-sea operations of a research vessel

Xiaobi M. Kuang[a], John A. Scott[a], Gisele O. da Rocha[a,b], Raghu Betha[c], Derek J. Price[c], Lynn M. Russell[c], David R. Cocker[d], and Suzanne E. Paulson[a]

[a]Department of Atmospheric and Oceanic Sciences, University of California–Los Angeles, Los Angeles, California, USA; [b]Instituto de Química, Universidade Federal de Bahia, Bahia, Brazil; [c]Scripps Institution of Oceanography, University of California San Diego, La Jolla, California, USA; [d]Bournes College of Engineering, Center for Environmental Research and Technology, University of California–Riverside, Riverside, California, USA

ABSTRACT

Reactive oxygen species, including hydroxyl radicals generated by particles, play a role in both aerosol aging and PM2.5 mediated health effects. We assess the impacts of switching marine vessels from conventional diesel to renewable fuel on the ability of particles to generate hydroxyl radical when extracted in a simulated lung lining fluid or in water at pH 3.5, for samples of engine emissions from a research vessel when operating on ultra-low sulfur diesel (ULSD) and hydrogenation-derived renewable diesel (HDRD). Samples were collected during dedicated cruises in 2014 and 2015, including aged samples collected by re-intercepting the ship plume. After normalizing to particle mass, particles generated from HDRD combustion had slightly to significantly (5–50%) higher OH generation activity than those from ULSD, a difference that was statistically significant for some permutations of year/fuel/engine speed. Water soluble trace metal concentrations and fuel metal concentrations were similar, and compared to urban Los Angeles samples lower in soluble iron and manganese, but similar for most other trace metals. Because PM mass emissions were higher for HDRD, normalizing to fuel increased this difference. Freshly emitted PM had lower activity than the "plume chase" samples, and samples collected on the ship had lower activity than the urban reference. The differences in OH production correlated reasonably well with redox-active transition metals, most strongly with soluble manganese, with roles for vanadium and likely copper and iron. The results also suggest that atmospheric processing of fresh combustion particles rapidly increases metal solubility, which in turn increases OH production.

1. Introduction

To reduce carbon emissions and their effects on global warming and ocean acidification, conversion of marine vessels to fuels derived from renewable (plant-based) sources could be a reasonable alternative to fossil fuel-based diesels, such as ultra-low sulfur diesel or ULSD. Hydrotreating of vegetable oil has been shown to produce a renewable biodiesel (hydrogenation-derived renewable diesel or HDRD; also referred to as hydrogenated vegetable oil or HVO) that is more compatible with many existing diesel engines than other untreated biofuels (Aatola et al. 2008; Heikkilä et al. 2012; Westphal et al. 2013; Kim et al. 2014; Prokopowicz et al. 2015; Bugarski et al. 2016). However, there is little information on whether using HDRD instead of ULSD in marine vessels would improve or exacerbate health effects in and near port areas. Clearly both HDRD and ULSD are improvements over the heavy fuel oil (HFO) currently in wide use in ocean transport. While currently they comprise a small fraction of fuel used for ocean transport, ULSD and similar cleaner fuels are currently required inside the 200 mile zone around the coastal United States, in major shipping lanes and ports throughout Europe, and in other areas, HFO is scheduled for global phase-out in 2020 (ICCT 2014). Shipping-related particle emissions have been estimated to be responsible for nearly 60,000 deaths annually (Corbett et al. 2007). Although the mechanisms for most of these deaths is

---

unknown, inhaled PM is thought to induce oxidative stress via biochemical reactions mediated by reactive oxygen species (ROS; Dellinger et al. 2001; Baulig et al. 2003), and oxidative stress is believed to underlie a number of diseases related to particulate matter (PM) inhalation (Li et al. 2003; Diaz et al. 2013). ROS are a class of reactive oxygen-bearing compounds that include the hydroxyl radical (OH), hydrogen peroxide (H_2O_2) and superoxide (O_2^-), and related species.

A handful of studies have examined the ability of diesel PM to produce ROS and pro-inflammatory responses in both cellular and a-cellular assays (Baulig et al. 2003; Cheung et al. 2009; Verma et al. 2010; Wang et al. 2012). Baulig et al. (2003) showed that the pro-inflammatory response of bronchial epithelial cells was induced by polycyclic aromatic hydrocarbon (PAH)-related compounds associated with the diesel exhaust particles. The response was further shown to be reduced by the addition of antioxidants, suggesting that the response to the PM is due to the presence of species in the particles that produce ROS. Verma et al. (2010) assessed the contribution of water-soluble transition metals present in diesel exhaust to the formation of reactive oxygen species (ROS), using a macrophage-based *in vitro* assay to determine the ROS activity of collected particles. Results indicated that soluble metals, especially Fe but also Cr, Co, and Mn accounted for a significant fraction of the ROS activity. Cheung et al. (2009) used the dithiothreitol assay to examine ROS production from biodiesel and conventional diesel particles, and found relationships with organic carbon, including both water-soluble and water-insoluble fractions. The biodiesel particles had significantly more ROS formation activity than the diesel particles. Wang et al. (2012) found that diesel and biodiesel particles from a diesel generator produced similar H_2O_2 formation, in both cases at much higher levels than urban ambient particles. H_2O_2 is one of the precursors to OH formation, however it is measured in steady state, rather than cumulatively as is OH, thus the H_2O_2 is more sensitive to species that can destroy it, such as free iron.

Several studies have reported that HDRD combustion results in lower PAH emissions than diesel fuel (Heikkilä et al. 2012; Jalava et al. 2012; Westphal et al. 2013). Westphal et al. (2013) further accessed the potential toxicity of diesel, hydrotreated vegetable oil, and other biodiesel fuels using *Salmonella typhimurium* strains, which are particularly sensitive to mutagens in organic extracts of diesel exhaust particles. Results showed that the mutagenicity of the HDRD emissions was the lowest compared to all other fuels tested. Furthermore, Jalava et al. (2012) collected PM from a EURO IV automobile engine powered by different fuel and performed inflammation,

cytotoxicity and cell apoptosis analyses, and ROS production using an intracellular dichlorofluorescein (DCFH) assay. In most cases, HDRD showed lower toxic potencies than conventional diesel fuel. While studies on HFO particulate emissions are few, in a recent and thorough study using lung epithelial cells and other analyses, Oeder et al. (2015) found that HFO particulate emissions had higher metal and organic content but lower black carbon content in comparison to conventional diesel emissions. Consistent with the relationships between ROS production, inflammation, and transition metals, Oeder et al. (2015) also found that HFO particles had much higher inflammatory responses than conventional diesel emissions.

ROS, and particularly the hydroxyl radical investigated here, can also mediate particle aging processes in ambient aerosols and cloud drops. Aerosol aging plays an important role in modifying aerosol chemical composition (Shrivastava et al. 2008; Sato et al. 2011; Donahue et al. 2012), hygroscopicity (Zhang et al. 2008; Buchholz et al. 2009), cloud condensation nuclei activity (Shilling et al. 2007; Engelhart et al. 2008; Wang et al. 2010), and optical properties (Reid et al. 1999). While much of the aerosol aging is likely mediated by heterogenous reactions of OH radicals from the gas phase, the contribution of reactions within the particles is not well understood. Similar ROS-mediated oxidation chemistry in cloud water may underlie some secondary organic aerosol (SOA) formation associated with cloud processing (Larsen et al. 2001; Zhang et al. 2010), some of this is photochemical, but the (dark) ROS chemistry probed here may be particularly important when photochemical processes shut down (Graedel et al. 1986). While ROS formation under physiological and environmental conditions is related, because of the differences in pH and concentrations of solutes, they are not necessarily well correlated.

Currently there are several assays available to measure ROS as a general class, as well as assays for specific ROS. General acellular assays include dichlorofluorescein (King and Weber 2013), dithiothreitol (Fang et al. 2014), or antioxidant consumption (Godri et al. 2011). Each has a different and largely uncharacterized response to H_2O_2, OH, and O_2^-, etc. There are several assays for specific ROS assays such as OH (this work, DiStefano et al. 2009; Charrier and Anastasio 2011) and H_2O_2 (Arellanes et al. 2006; Shen et al. 2011). Differences in the assays and their sensitivities to specific ROS likely explain at least some of the differences in conclusions about which particulate matter components are responsible for ROS. A series of studies by Charrier, Anastasio and co-workers have provided many insights into the behavior of a series of contributors to ROS by quantifying differences in

responses to individual and pairs of transition metals and quinones to several individual antioxidants (Charrier and Anastasio 2011, 2012; Charrier et al. 2014), but there is more work to be done to develop an understanding of ambient aerosol behavior. Still uncertain are the roles of other variables including particularly organic/brown carbon but also pH, other solutes, and black carbon, as well as the concentrations of the reactants.

Here, we probe OH formation, which has been shown to be mediated by transition metals, with contribution from quinones (DiStefano et al. 2009; Charrier and Anastasio 2011). Other aerosol components are expected to influence OH formation by altering the activity of transition metals (Gonzalez et al. submitted), or other unknown mechanisms. We measure OH production and trace metal content of particle samples collected both from the engine stack and by intercepting the ship plume alternately on HDRD and ULSD fuels in 2014 and 2015. Samples were extracted either in simulated lung fluid (SLF) containing three antioxidants present in lung lining fluid: ascorbate, glutathione, and uric acid (Kelly et al. 1995; Charrier and Anastasio 2011), with citrate added to mimic transition metal chelating ability of proteins in lung fluid (Lund and Aust 1992; Smith and Aust 1997; Godri et al. 2011) or in water adjusted to pH 3.5 to probe *in situ* reactivity of the PM in marine air. Samples were analyzed for OH formation activity, water-soluble elements, PM and black carbon mass concentrations normalized to both particle mass and kg fuel burned. The measurements provide an evaluation of the changes in reactivity and soluble transition metals, under both physiological and environmental conditions, associated with switching fuels, and a measure of their reactivity compared to urban and mixed marine particulate matter.

Simultaneous measurements of particle and gas mass emission and chemical composition and concentrations are reported in two companion papers (Betha et al. 2017; Price et al. 2017). Betha et al. (2017) showed that emission factors for CO and NO_x were higher for ULSD than HDRD, and EFs decreased with increasing engine speed. Different trends were observed for black carbon and particle number, with higher number and mass emission factors for HDRD. The organic composition of particle-phase ship emissions from both fuels consisted of two types of hydrogen-like organic aerosol, one containing more saturated alkane fragments (diesel type) and the other more mono-unsaturated fragments (cooking type). The latter was more abundant in PM from HDRD. The ULSD aerosol emissions also contained significant oxidized organic material, while HDRD emission did not, although this result is based on a small number of samples of ULSD-derived PM. The aged plumes consisted of a larger contribution from sulfate (a major component of the marine background), and contributions from oxygenated and in some cases diesel-type hydrocarbon organic aerosol. Cooking-type aerosol was completely reduced or absent in HDRD aged plumes (Price et al. 2017).

2. Methods

During two dedicated sampling cruises in 2014 (29 September to 3 October) and 2015 (4 to 7 September and 26 to 28 September), the fuel tanks of the R/V *Robert Gordon Sproul* were filled with ultra-low sulfur diesel (ULSD) and hydrogenation-derived renewable diesel (HDRD), which were used alternately in the existing diesel engines. Properties of the HDRD and ULSD fuels used in this study are shown in Table S1. Since the ship was not equipped with an engine dynamometer, sampling was conducted at four engine speeds (1600 rpm, 1300 rpm, 1000 rpm, 700 rpm). Nonetheless, emissions at any engine speed did vary with sea state and other conditions (Betha et al. 2017). Simultaneous measurements of gas and particle emissions are described in companion papers (Betha et al. 2017; Price et al. 2017).

2.1. Particle collection

All samples subjected to ROS and related analyses were collected on pre-weighed, acid cleaned 47 mm Teflon filters (0.2 μm pore size, Pall Corp., Port Washington, NY, USA; Paulson et al. 2016). Prior to collection of each sample, the collection flow rate was checked using a digital mass flow meter (TSI). After collection, the filters were transported and stored in individual Teflon petri dishes sealed with Teflon tape and stored in a freezer at or below 0°C for later analysis. The mass of samples collected was determined gravimetrically by weighing the filters before and after sample collection using a micro-balance (1 μg precision, ME 5, Sartorius) in a temperature (22–24°C) and humidity (40–45%) controlled room, equipped with a sodium lamp to avoid interactions with light.

For the 2014 cruise, fresh emissions were collected directly from the ship stack using a Venturi probe (Nigam 2007) followed by a PM$_{2.5}$ cyclone operating at 16.05 LPM, for 15–20 min for each. A separate sampling van located on the aft deck equipped with a PM$_{2.5}$ cyclone (URG-2000-30ENB) operating at 92 LPM was used to collect 2015 samples as well as the 2014 mixed samples. Fresh emissions were collected as the vessel was moving so the travel time from the stack to the van inlet (a distance of approximately 20 m) was less than 30 s. These samples were much more diluted and cooled compared to the stack samples, and collection times were about 60 min. Additional samples were collected from re-intercepting the aged ship plume, and overnight

samples captured a mixture of ship emissions and marine background aerosols. Both types of samples are classified as "mixed" in the following sections primarily because there are too few to treat them separately.

To create full field blanks, able to detect contamination from anywhere along the sample train, blanks were collected in the same manner as the samples, by loading blank filters into the filter holders for 30 s. Very minimal to no detectable material was collected on the blank filters.

2.2. Analyses

2.2.1. Materials

Trifluoroethanol (TFE), sodium citrate tribasic dihydrate (Cit), L-ascorbic acid (Asc), uric acid sodium salt (UA), and L-glutathione reduced (GSH), 0.1 N sulfuric acid, and Chelex 100 sodium form (50–100 dry mesh) were purchased from Sigma Aldrich (St. Louis, MO, USA). Sodium phosphate dibasic and potassium phosphate monobasic were purchased from Acros Organics (Thermo Fisher, Waltham, MA, USA). Nitric acid (70% trace metal grade) was purchased from Fisher Scientific (Pittsburg, PA, USA). All materials were used as received.

2.2.2. Extraction solutions

Simulated lung fluid (SLF) was prepared by adding four antioxidants (Cit, Asc, UA, and GSH) at 100 μM UA and GSH, 300 μM Cit and 200 μM Asc, to phosphate buffer at pH 7.2–7.4. Phosphate buffer contained 114 mM of NaCl, 7.8 mM of sodium phosphate dibasic, and 2.2 mM of potassium phosphate monobasic, and was chelex-treated to remove trace metals prior adding the antioxidants. The antioxidants were freshly prepared in phosphate buffer for each experiment.

pH 3.5 solution was prepared by acidifying 18 MΩ deionized (DI) water using 0.1N sulfuric acid. The pH meter was calibrated prior to each use.

2.2.3. Trace metal cleaning and particle extraction

A rigorous cleaning process was followed for all glass and Teflon containers. After each use, each vessel was washed with warm water and soap, and then rinsed in deionized (18 MΩ-cm DI) water (3x), ethanol (3x), and finally DI water (3x). The vessels were then soaked in 1 M nitric acid bath overnight, rinsed with DI water, and air dried. Nitric acid baths were replaced after being used twice and kept covered to avoid dust deposition. All analytical solutions were prepared with 18 MΩ-cm DI water that had been passed through a chelex column to remove trace metals.

Filters were cut in half using a cleaned ceramic blade. Half filters were extracted in 6 mL SLF or pH 3.5 solution in Teflon petri dishes with gentle agitation. To increase particle solubility, the filters were wetted first with 50 μL of trifluoroethanol.

2.2.4. Hydroxyl radical quantification

OH formation by PM was monitored by adding excess (10 mM) sodium terephthalate (TA) to extraction solutions and allowing it to react for 2 h. 2-hydroxytereph-thalic acid (TAOH), a strongly fluorescent product, is produced from the OH reaction with TA with 33% yield at pH 7.2 and 31% at pH 3.5 (Matthews 1980). TAOH is detected at excitation/emission wavelength ($\lambda_{ex}/\lambda_{em}$) of 320/420 nm using a fluorometer (Lumina, Thermo Scientific), resulting in a detection limit of about 10^{-10} M. The microcuvettes were cleaned with water and ethanol and dried between each sample measurement. Calibrations were performed daily. To verify the PM did not interfere with our assay, extracts of PM and fuel samples were scanned and observed to have no native fluorescence over any wavelengths of interest.

Many ROS assays have unequal sensitivities to different sources and types of ROS. In some cases, the probe interacts directly with one or more of the metals, potentially changing its redox activity, as in the case for benzoate and Mn (Charrier and Anastasio 2011). We have carefully examined the terephthalate assay for iron and copper; its response to iron is in excellent agreement with well-known Fenton and related chemistry for iron (Gonzalez et al. submitted), and we additionally verified that the interactions between copper observed at high concentrations and terephthalic acid (Cardarelli et al. 1979) do not take place at the lower concentrations observed here (Kuang et al. in preparation).

2.2.5. Water-soluble metals

Due to limited numbers of samples, soluble element analysis was only performed on samples extracted in SLF. Aliquots from extraction solutions after 2 h were filtered through 0.2 um polypropylene syringe filters (VRW International) and then acidified to 2% (by weight) with HNO_3, and stored in 15 mL Falcon conical centrifuge tubes. An Agilent 8800 Triple Quadrupole ICP-MS was used to measure the following elements and transition metals in the MS/MS mode: Mg, S, K, Ca, V, Cr, Mn, Fe, Co, Ni, Cu, Zn, Se, Cd, La, Pb. Calibration curves were made from a 10 ppm 33 multi-element standard (SCP Science), using ^{89}Y as an internal standard (Inorganic Ventures MSY-100PPM) to correct for matrix effects. Five replicate measurements were averaged for each individual sample. All reported metals were well above their detection limits. The average variation between replicate measurements of the same sample was 1.3%, and it never exceeded 5% for any individual sample.

Fuel samples were collected from the tank truck as the fuel was pumped into the research vessel. A micro-emulsion technique following the ICP manufacturer's protocol was used to dissolve crude oil into a water matrix. 1% of crude oil was mixed with 1% of the surfactant TRITON-X100 (Electrophoresis Grade, International Biotechnologies Inc.) and sonicated for 60 min, and then analyzed for metals following the above procedures.

2.2.6. Black carbon quantification

Black carbon was quantified using an OT21 duel wavelength optical transmissometer (Magee Scientific Corporation). A quartz diffuser backing (Pallflex Fiberfilm) was placed under each 47 mm Teflon filter to provide an even distribution of light to the detector. Absorption at 880 nm is proportional to the concentration of black carbon (Hansen et al. 1984) expressed by the following equation:

$$[BC] = \frac{b_{ATN}}{\sigma(\lambda)_{ATN}}, \quad [1]$$

where b_{ATN} is the attenuation coefficient and $\sigma(\lambda)_{ATN}$ (m^2/g) is the specific attenuation cross section. The EPA empirically determined $\sigma(\lambda)_{ATN}$ value of 16.6 $m^2 g^{-1}$, suggested by the manufacturer for engine derived BC, was used for this calculation.

3. Results

3.1. OH formation in SLF

The number of samples analyzed for each fuel and year, together with the numbers of samples analyzed for soluble elements is summarized in Table 1. Figure 1a shows the averages, medians, and standard errors (1σ) for OH production in SLF, normalized to aerosol mass, by year and fuel. Most of the sample sets included one or two samples with much higher activity than the others,
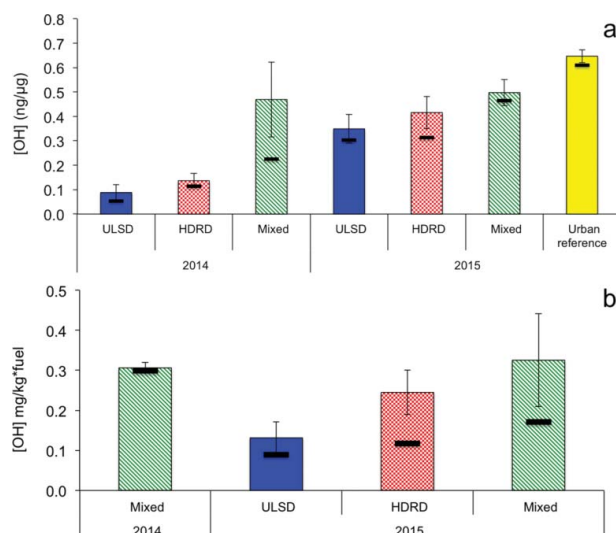

Figure 1. (a) Average (color bar), median (black horizontal bar), and standard errors (vertical error bars) of OH (ng/μg PM) production by year and fuel (1a) and average and standard error of OH (mg/kg•fuel) in (b). ULSD and HDRD are the samples from engine cycle tests, with all of the engine speed combined.

resulting in a high degree of sample variability, thus medians may be a better metric than averages.

OH production normalized to kilograms of fuel burned is shown in Figure 1b. Values are shown only for 2015, as in 2014 stack sample CO_2 measurements were not available due to instrument problems (Betha et al. 2017). Consistent with the observation that PM mass emissions were higher for HDRD than ULSD (Betha et al. 2017), once normalized to fuel burned, the differences between 2015 ULSD and HDRD OH generation activity is larger than the PM-mass normalized data.

For both fuels, the 2015 samples had higher activity than the 2014 samples. The averages of the HDRD samples were higher than the ULSD samples for both years (Figure 1a, Table S2), and medians were higher for 2014

Table 1. Number of samples analyzed for ULSD and HDRD in 2014 and 2015 cruises. Numbers in parentheses indicate the number of metal samples analyzed and bolded values indicate average aerosol mass in mg.

2014 Cruise		1600 rpm	1300 rpm	1000 rpm	700 rpm	Total
ULSD	SLF	4 (2) **0.69**	3 (1) **0.26**	1 **0.18**	2 (1) **0.25**	10 **0.42**
	pH3.5	2 **0.82**	2 **0.24**	1 **0.18**	2 **0.25**	7 **0.40**
HDRD	SLF	2 (1) **1.00**	2 (1) **0.32**	2 (2) **0.10**	2 (1) **0.15**	8 **0.39**
	pH3.5	1 **1.63**	1 **0.40**		1 **0.18**	3 **0.74**
Mixed	SLF	3 (2) ULSD **0.51**	5 (2) HDRD **0.61**			8 **0.57**
	pH3.5	2 **0.18**				1
2015 Cruise		1600 rpm	1300 rpm	1000 rpm	700 rpm	Total
ULSD	SLF	2 (1) **0.09**	2 (1) **0.11**	2 (1) **0.11**	3 (2) **0.09**	9 **0.10**
	pH3.5	1 **0.04**	1 **0.03**	1 **0.04**	1 **0.06**	4 **0.04**
HDRD	SLF	6 (5) **0.05**	6 (5) **0.06**	7 (6) **0.10**	7 (6) **0.09**	26 **0.08**
	pH3.5	1 **0.03**	1 **0.05**	1 **0.08**	1 **0.12**	4 **0.07**
Mixed	SLF	3 (3) ULSD **0.03**	11 (9) HDRD **0.07**			14
	pH3.5	1 **0.09**				

but almost identical for 2015. Differences were significant ($p < 0.05$) for 2014 averages and medians on a PM mass basis (Figure 1a), and 2015 averages on a per kg fuel basis (Figure 1b). OH production from PM in mixed/aged ship samples was much higher than the fresh samples, and all samples in this study were significantly lower than average OH formation for Los Angeles urban air samples analyzed with the same techniques (Paulson et al. 2016). Relationships with chemical composition of the particle are presented below.

Figure S1a shows OH production in SLF separated by fuel, year, and engine speed. While most engine condition and fuels were tightly clustered, frequently a single sample from a set was higher by a factor of 3 or more than the comparison samples. Thus, when separated by engine speed, none of the conditions are different at the 95% confidence level. For HDRD, OH generation increased at lower engine speed, while for ULSD there was a slight decrease as engine speed was lowered.

3.2. Relationship between OH formation and PM mass

For combined 2014 and 2015 data, OH formation by particles was not correlated to mass. However, for the ULSD, HDRD, and mixed subsets of the 2014 data, OH formation was strongly correlated with mass (Figure S2). The 2015 data (which had much lower masses) still showed little or no correlation with mass when separated by sample type (Figure S2). 2014 fuel-specific slopes were 1.4, 2.7, and 5.5, for ULSD, HDRD, and mixed samples, respectively (adjusted r^2 of 0.34 to 0.96, Figure S2). Similar trends were observed for OH activity vs. absorbance at 880 nm (a proxy for black carbon) for the 2014 samples (Figure S3), measured on the filters by transmissometer; 2015 filters had too little absorbance for accurate measurement of BC. The clearly differentiated behavior of different sets of samples indicates that components (such as transition metals) other than total mass, BC, and/or associated organics are driving factors in OH production, consistent with results presented below.
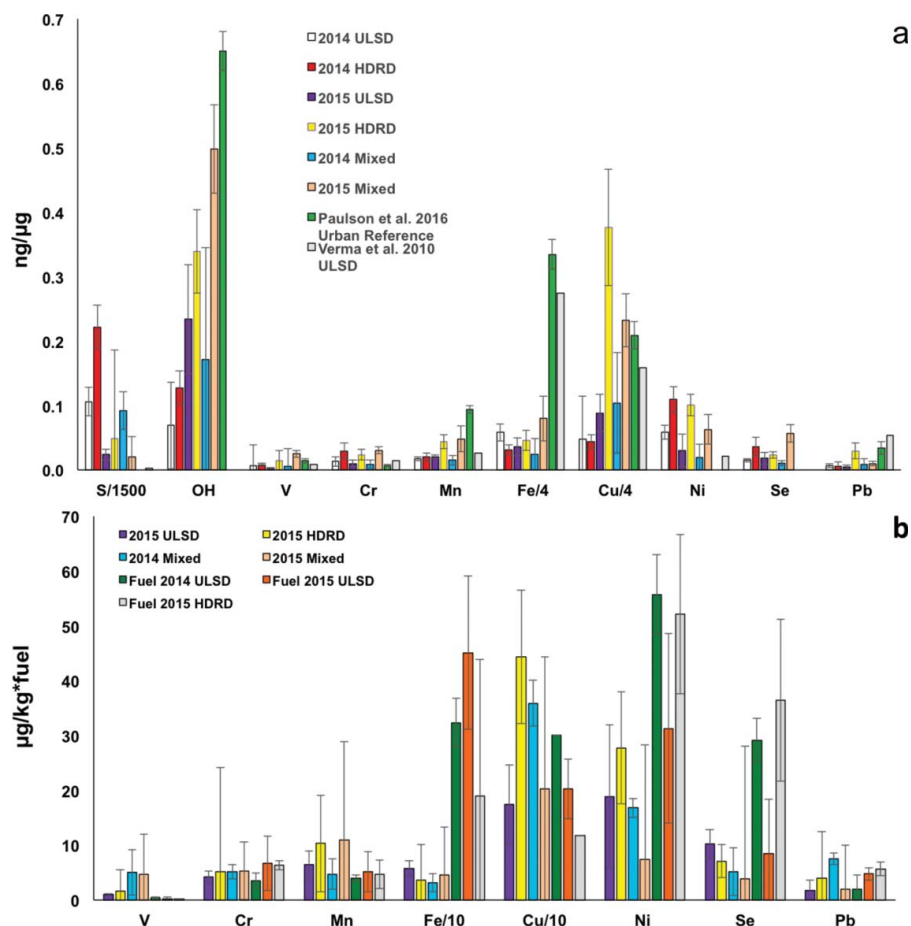
Figure 2. (a) ICP-MS/MS concentrations of water-soluble transition metals in the exhaust PM (in ng metal or element/μg PM), S and Se in the ship samples, an urban data set (Paulson et al. 2016) and in diesel engine exhaust (Verma et al. 2010). All samples were extracted in SLF solution (see the text) except Verma et al. (2010), who used water. Note that there are somewhat fewer samples with metal analysis than OH (Table 1), thus the average OH generation for the corresponding sample set is included here. (b) Concentrations of water-soluble transition metals in the ship exhaust (μg metal per kg of fuel burned) and in the fuels (μg metal per kg of fuel).

3.3. Water-soluble trace metals

Median concentrations and standard errors for transition metals, sulfur, and selenium in the ship samples extracted in SLF are shown in Figure 2a. 68% of SLF-extracted samples were analyzed for trace metals, thus corresponding OH production for this subset of samples, with slightly different values from Figure 1a, is also shown in Figure 2a. The metal concentrations for a Los Angeles urban data set, analyzed with the same methods (Paulson et al. 2016) are also included for reference, as well as metal concentrations for fresh diesel PM collected from a school bus and extracted in water by Verma et al. (2010).

All soluble PM metal concentrations in the ship samples were in the same range as the urban and bus emission PM concentrations (Figure 2a). Compared to the urban concentrations, ship PM had similar V, similar or slightly higher Ni, Cr, and Se, and lower Mn and Fe. Cu and Pb were lower in the ship PM except in the case of 2015 HDRD, which had markedly higher Cu and Pb than the other ship samples. Concentrations of V, Cr, and Mn in the ULSD ship emissions were similar to those observed by Verma et al. (2010) for conventional diesel emissions while Cu, Fe, and Pb were much lower. For all ship samples except 2015 ULSD, sulfur was much higher than the bus emissions. The 2014 stack samples generally had lower soluble metal concentrations than the 2015 samples. While the reasons for this are not clear, it may be related to the lack of even minimal atmospheric processing of the particles in the stack samples, differences in OM content (unfortunately the OM content was not measured in the 2014 stack samples due to an instrument issue). It could also possibly stem from an artifact from the stack dilution system, such as size-dependent sampling losses in the Venturi inlet.

Few other reports of soluble transition metals in related samples are available. Jalava et al. (2012) reported trace metal concentrations, in PM from a heavy-duty Euro IV engine on a chassis dynamometer burning HDRD and ULSD (En590) extracted in aqueous 0.08N HNO_3. Compared to our 2015 HDRD values, they observed lower Cu, V, Ni, and Pb (4–23% of our values), and Cr at 124%, Mn at 54%, and Fe at 232% (not shown in Figure 2 for clarity). For reference, the Jalava et al. (2012) ULSD trace metal concentrations were 55–243% of the values reported by Verma et al. (2010) except V and Pb, which were 21 and 6%, respectively. Jalava et al. (2012) found slightly lower intercellular ROS activity for HDRD in comparison to ULSD PM, consistent with the slightly lower transition metals in the HDRD compared to the ULSD PM.

Figure 2b shows the 2015 mass of soluble metals per kg of fuel, as well as the mass of metals per kg of fuel for three of the fuels used in this study, 2014 and 2015 ULSD and 2015 HDRD. Generally, the trace metal PM concentrations shown in Figure 2b (Cr, Cu, Fe, Mn, Pb, Se, and V) are in reasonably good agreement with the corresponding fuel values, averaging 146 and 242% for ULSD and HDRD, respectively. V is much higher in the PM for both fuels, Mn and Cu are somewhat higher in the PM, and Fe is much lower, Ni and Pb are lower in PM than the fuels, while Cr for both fuels and Se in ULSD are similar (Figure 2b and Table S3), although none of the differences are significant given the variability in the measurements. If V is excluded, the PM from ULSD and HDRD average 79 and 131% of the fuel values. Overall however, given the scatter in the data, too much should not be made of the differences. There are several potential sources of differences between fuel and PM metal concentrations, including engine wear (Agarwal et al. 2003), lubricating oil, and deposition within the engine (Wang et al. 2003). We were not able to measure metals in the lube oil as part of the study. Metals in lube oil have been reported to be dominated by non-redox active oil additives such as Ca, Zn, and P (Agarwal et al. 2010) and to account for <1% of the resulting total PM mass (Storey et al. 2015). The lower concentrations of Fe in the fuel and PM may be due to losses of Fe in the engine, but they may also be explained by a significant portion of the Fe in the PM being in an insoluble form. Fe forms many complexes and tends to be less soluble especially at higher pHs than many other transition metals (Deguillaume et al. 2005).

In comparison to fresher PM, trace element concentrations in plume chase and nighttime samples (labeled "mixed," Figure 2) were higher for 2015 V, Mn, Fe, Se, and Cu and in 2014 for Cu; other elements were similar except 2014 Fe, which was lower. OH formation in the mixed samples was higher than the corresponding fresh samples, consistent with the higher concentrations of soluble redox active metals, and suggesting metal solubility increases rapidly as aerosols are aged. Evidence for increasing ROS production as fresh combustion aerosols are aged, although not necessarily directly linked to metal solubility, has also been provided by McWhinney et al. (2013), Li et al. (2009), and Rattanavaraha et al. (2011).

We were unfortunately not able to collect pure marine background filter samples, however online measurements indicated very low PM mass concentrations in the marine boundary layer, less than about 0.5 $\mu g/m^3$ (Price et al. 2017), compared to average mass concentrations in

Table 2. Cross correlations between elements (r^2 values), mass normalized in ng/μg. Significant correlations ($p < 0.05$) are in bold; italic values indicate a group of metals that all have significant correlations with one another. n indicates the number of samples.

All Fuels, R^2	S	V	Cr	Mn	Fe	Cu	Se	Pb	Co	Ni	n
S	1	0.04	0.01	0.05	0.04	0.10	0.002	0.005	0.001	**0.30**	44
V		1	0.04	**0.07**	0.01	**0.11**	**0.07**	0.06	0.007	**0.16**	57
Cr			1	0.2	**0.10**	**0.11**	**0.10**	0.02	**0.570**	**0.18**	57
Mn				1	*0.47*	*0.61*	0.22	*0.29*	0.070	*0.47*	58
Fe					1	*0.11*	0.16	0.15	0.010	*0.17*	56
Cu						1	0.09	*0.50*	0.020	**0.49**	57
Se							1	0.04	0.010	0.12	51
Pb								1	0.010	*0.14*	55
Co									1	0.04	58
Ni										1	57

the mixed samples above 15 μg/m³. Metals in marine aerosols have been reported in a few instances (Baker et al. 2013; Chance et al. 2015) but these studies did not report aerosol mass, and extracted in organic solvent, so it is difficult to compare with these measurements.

For the whole dataset, some soluble elements were fairly strongly correlated with one another (Table 2), including Cr and Co ($R^2 = 0.57$), Mn and Fe ($R^2 = 0.47$), Mn and Cu ($R^2 = 0.61$), and Cu and Pb ($R^2 = 0.50$). Additionally, Mn, Fe, Cu, and Pb were all cross-correlated with one another at the $p < 0.05$ level. Divided by fuel, there are a handful of strong correlations, but no consistent patterns for ULSD or HDRD between the 2 years (not shown). S and V are commonly used as tracers of ships burning high sulfur fuels such as bunker fuel (BluewaterNetwork 2000; Lin et al. 2005; Arhami et al. 2009). The much cleaner ULSD and HDRD used here did not consistently produce high S and produced little V emissions. Further, the ratio of V/Ni was less than one, similar to on-road diesel engine exhaust (Lin et al. 2005) rather than above 1.5, the expected value for heavy oil marine fuels (Arhami et al. 2009).

3.4. Relationships between OH generation and transition metals

Overall, OH has reasonably strong single variable correlations with transition metals, after controlling for mass (Table 3); mass normalization is necessary for this dataset because the 2014 ship stack samples had much higher masses than the 2015 van samples (Table 1). The correlations were strongest for Mn ($R^2 = 0.52$) followed by Co,

Cu, and V all ($R^2 = 0.37$–0.41), and significant ($p < 0.05$) for Fe and Se, as well as Pb, Ni, and Mg. Mn, Cu, Fe, and V have all been shown to produce OH in SLF in other studies (DiStefano et al. 2009; Charrier and Anastasio 2011; Gonzalez et al. submitted; Paulson et al. 2016); cobalt and the other elements are not expected to be redox active under our conditions (Table 2). The correlation analyses are confounded by significant co-linearities, as well as large differences in other components in the particles, including BC and organic material (Figure 3 and Price et al. 2017).

Multivariate analysis of all data resulted in the correlation shown in Figure S4; the only combination for which the independent variables were all significant (at $p < 0.05$; here $p < 10^{-3}$ for both Mn and V) includes only Mn and V. Co-linearity tends to reduce the apparent significance of other variables, thus this result should not be interpreted as ruling out a role for other trace metals. Based on the single variable correlations combined with results from other studies (DiStefano et al. 2009; Charrier and Anastasio 2011; Gonzalez et al. submitted; Paulson et al. 2016) and many others, it is likely that iron and copper also contribute to OH formation here.

3.5. Relationships between OH and other chemical components

Figure 3 shows overall chemical composition of the particles using all data measured in all samples. "Metals" is dominated by Ca, followed by Mg and Zn (Table S2), none of which are included in Figure 2, as these are not expected to be redox active. While soluble trace metal

Table 3. Correlations between OH and metals mass normalized in ng/μg. Bolded values indicate the significant correlations with p values < 0.05. Italic values indicate that outliers (one for Fe, two each for Ca and Co) were removed. Outliers are defined as the values at least three times higher than the next highest value.

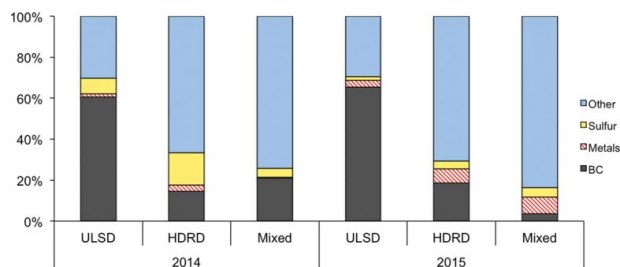|	Ca	Mg	S	V	Cr	Mn	Fe	Cu	Se	Pb	Co	Ag	Ni
N	57	59	44	57	57	58	56	57	51	55	58	45	58
R^2	*0.12*	0.25	**0.03**	**0.37**	**0.40**	**0.52**	*0.23*	**0.40**	0.23	**0.32**	*0.41*	0.08	**0.28**
Slope	0.002	0.01	-	2.93	5.75	3.42	0.37	0.13	4.98	2.16	44.3	-	1.95

Figure 3. Median chemical composition of different sample types. Total "Metals" includes 13 metals and Se, but was dominated by Mg, Ca, and Zn (Table S2). BC mass concentrations in all 2014 samples were measured with an Aethalometer (Paulson et al. 2016) and BC mass concentrations in 2015 samples were measured with an SP2 (Betha et al. 2017).

concentrations (Figures 2 and 3) can explain a reasonable amount of the observed variability in OH formation among sample types, the data imply other components are also important. By sample type, OH production generally increases with increasing redox active transition metals, e.g., the sum of Mn, Cu, Fe, and V (Figure 2a). However, close examination of the data in Figure S4 shows differences in slopes between sample types; the ULSD slopes are both lower than other data, especially for 2015. These differences may be related to the marked differences in BC content (Figure 3) and in the composition of the organic fraction. In both years, HDRD samples had a smaller fraction of BC in comparison to the ULSD samples. The organic material in the ULSD and HDRD PM was also different; the ULSD particles contained more diesel-type hydrocarbon-like organic aerosol (HOA), while HDRD had more cooking-type HOA (Price et al. 2017). Mixed samples (aged in Price et al. 2017) were more depleted in cooking-type HOA. Organic interactions with metals have been shown repeatedly to be capable of enhancing transition metal solubility (Sun and Pignatello 1992; Weng et al. 2002; Paris and Desboeufs 2013), and differences in organics may be responsible for the higher concentrations of soluble metals and higher OH production in the HDRD and mixed samples, although lower BC could also play a role. The only organic characteristics for
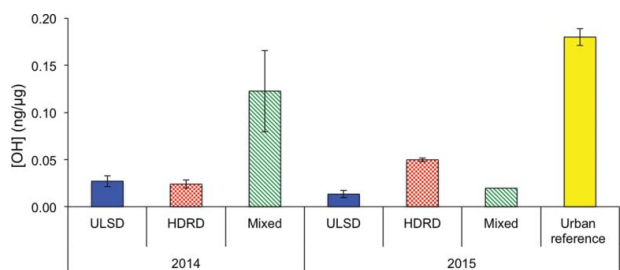
which we had sufficient data to perform a regression, the O/C and H/C ratio, were not correlated with OH formation. However, the strong correlations of OH with the several of the metals, may mask more moderate relationships with other characteristics. The sample set (and subsets) for which we have complete data for OH, elements, O/C and H/C, and BC are unfortunately not sufficiently overlapping to perform a multivariate analysis that includes transition metals together with any of the carbon-based variables, thus further testing of this hypothesis is not possible with this dataset.

3.6. pH 3.5: OH production under atmospherically relevant conditions

OH production by ULSD and HDRD PM emissions was also measured by extracting particles in water at pH 3.5, to mimic acidic aerosol liquid water and nascent cloud water particles (Figure 4). In all cases, activity of the fresh emission samples and the plume chasing samples was substantially smaller than the urban reference data by a factor of 8 ± 4. Similar to SLF extraction, the most active samples were the 2015 HDRD emissions, however in contrast to SLF the pH 3.5 2014 HDRD had slightly lower activity than the ULSD.

OH production averaged 4 ± 2 times lower in pH 3.5 compared to SLF extraction solution. The differences between OH production in SLF and pH 3.5 solutions are likely largely driven by two factors: the pH dependence of metal solubility, and the availability of antioxidants to chelate metals and/or act as electron donors. Metals such as manganese and copper are already fairly soluble at high pH, while iron solubility increases dramatically between pH 7.2 and 3.5 (Deguillaume et al. 2005). Charrier and Anastasio (2011) showed that in simplified solutions, one of the antioxidants, ascorbate, can enhance OH formation by more than two orders of magnitude for some metals (particularly Fe, Cu, and V). This enhancement was strongly moderated by glutathione and citrate in the solution for Cu and V, but further enhanced for iron. Benzoate, the OH probe used in that study interacts with manganese, so the effect of SLF solutes is not well understood for Mn. These aerosols also contain substantial amounts of black and organic carbon, and this material is also expected to influence OH formation in ways that are pH dependent. For example, the chelation activity of carboxylic acid groups present in complex organic molecules is pH dependent (Tan 2014).

4. Discussion and conclusions

The results indicate a large fraction of OH generation is controlled by soluble redox-active transition metals,

Figure 4. Average and standard error of OH production divided by fuel and year in pH 3.5. The 2015 mixed bar contains only one data point, and 2014 contains two.

and are further consistent with the notion that metal solubility increases rapidly as freshly emitted particles are released into the marine boundary layer, which in turn increases OH formation. Concentrations of trace metals in the PM emissions appear to be largely due to trace metals in the fuels, although there may also be a significant contribution from lubricating oil or from the engine itself. OH formation and soluble metals were as high or higher in HDRD compared to ULSD emissions.

Simultaneous measurements of particle chemical composition and concentrations show that the mass and number of particles also increase in HDRD compared to ULSD engine emissions (Betha et al. 2017; Price et al. 2017). Taken together, these measurements indicate that switching fuels may result in particles that are as or more harmful to human health. However, due to the variability of the results between samples and engine conditions, these results should be verified with additional sampling under a variety of sea and ship conditions.

Acknowledgments

Funding

References

Aatola, H., Larmi, M., Sarjovaara, T., and Mikkonen, S. (2008). Hydrotreated Vegetable Oil (HVO) as a Renewable Diesel Fuel: Trade-Off between NOx, Particulate Emission, and Fuel Consumption of a Heavy Duty Engine. *SAE Paper*:2500.

Agarwal, A. K., Bijwe, J., and Das, L. (2003). Effect of Bio-diesel Utilization of Wear of Vital Parts in Compression Ignition Engine. *J. Eng. Gas Turbines Power*, 125:604–611.

Agarwal, A. K., Gupta, T., and Kothari, A. (2010). Toxic Potential Evaluation of Particulate Matter Emitted from a Constant Speed Compression Ignition Engine: A Comparison Between Straight Vegetable Oil and Mineral Diesel. *Aerosol Sci. Technol.*, 44:724–733.

Arellanes, C., Paulson, S. E., Fine, P. M., and Sioutas, C. (2006). Exceeding of Henry's Law by Hydrogen Peroxide Associated with Urban Aerosols. *Environ. Sci. Technol.* 40 (16):4859–4866

Arhami, M., Sillanpää, M., Hu, S., Olson, M. R., Schauer, J. J., and Sioutas, C. (2009). Size-Segregated Inorganic and Organic Components of PM in the Communities of the Los Angeles Harbor. *Aerosol Sci. Technol.*, 43:145–160.

Baker, A., Adams, C., Bell, T., Jickells, T., and Ganzeveld, L. (2013). Estimation of Atmospheric Nutrient Inputs to the Atlantic Ocean from 50° N to 50° S Based on Large-Scale Field Sampling: Iron and Other Dust-Associated Elements. *Global Biogeochem. Cycles*, 27:755–767.

Baulig, A., Garlatti, M., Bonvallot, V., Marchand, A., Barouki, R., Marano, F., and Baeza-Squiban, A. (2003). Involvement of Reactive Oxygen Species in the Metabolic Pathways Triggered by Diesel Exhaust Particles in Human Airway Epithelial Cells. *Am. J. Physiol.-Lung Cell. Mol. Physiol.*, 285:L671–L679.

Betha, R., Sanchez, K. J., Liu, J., Price, D. J., Lamjiri, M. A., Chen, C.-L., Kuang, X. M., da Rocha, G. O., Paulson, S. E., Miller, J. W., Cocker, D. R., and Russell, L .M. (2017). Lower NOx but Higher Particle and Black Carbon Emissions from Renewable Diesel compared to Ultra Low Sulfur Diesel in At-Sea Operations of a Research Vessel. *Aerosol Sci. Technol.*, 51(2):123–134.

Bluewater Network. (2000). *A Stacked Deck: Air Pollution from Large Ships*. Georgia Strait Alliance, San Francisco, CA. Available at https://georgiastrait.org/wp-content/uploads/2015/03/StackedDeck.pdf (accessed 15 July 2016).

Buchholz, A., Mentel, T. F., Tillmann, R., Schlosser, E., Mildenberger, K., Clauss, T., Henning, S., Kiselev, A., and Stratmann, F. (2009). Photochemical Aging of Secondary Organic Aerosols: Effects on Hygroscopic Growth and CCN Activation, in EGU General Assembly Conference Abstracts, 11:8288.

Bugarski, A. D., Hummer, J. A., and Vanderslice, S. (2016). Effects of Hydrotreated Vegetable Oil on Emissions Of Aerosols and Gases from Light-Duty and Medium-Duty Older Technology Engines. *J. Occup. Environ. Hyg.*, 13:293–302.

Cardarelli, E., D'Ascenzo, G., Magri, A., and Pupella, A. (1979). Complexes of Cobalt (II), Nickel (II) and Copper (II) with the Benzenedicarboxylic Acids. *Therm. Prop.. Thermochim. Acta*, 33:267–273.

Chance, R., Jickells, T. D., and Baker, A. R. (2015). Atmospheric Trace Metal Concentrations, Solubility and Deposition Fluxes in Remote Marine Air Over the South-East Atlantic. *Marine Chem.*, 177:45–56.

Charrier, J. G., and Anastasio, C. (2011). Impacts of Antioxidants on Hydroxyl Radical Production from Individual and Mixed Transition Metals in A Surrogate Lung Fluid. *Atmos. Environ.*, 45:7555–7562. DOI: 10.1016/j.atmosenv.2010.12.021.

Charrier, J. G., and Anastasio, C. (2012). On Dithiothreitol (DTT) as a Measure of Oxidative Potential for Ambient Particles: Evidence for the Importance of Soluble Transition Metals. *Atmos. Chem. Phys. (Print)*, 12:11317–11350. DOI: 10.5194/acpd-12-11317-2012.

Charrier, J. G., McFall, A. S., Richards-Henderson, N. K., and Anastasio, C. (2014). Hydrogen Peroxide Formation in a Surrogate Lung Fluid by Transition Metals and Quinones

Present in Particulate Matter. *Environ. Sci. Technol.*, 48:7010–7017. DOI: 10.1021/es501011w.

Cheung, K. L., Polidori, A., Ntziachristos, L., Tzamkiozis, T., Samaras, Z., Cassee, F. R., Gerlofs, M., and Sioutas, C. (2009). Chemical Characteristics and Oxidative Potential of Particulate Matter Emissions from Gasoline, Diesel, and Biodiesel Cars. *Environ. Sci. Technol.*, 43:6334–6340.

Corbett, J. J., Winebrake, J. J., Green, E. H., Kasibhatla, P., Eyring, V., and Lauer, A. (2007). Mortality from Ship Emissions: A Global Assessment. *Environ. Sci. Technol.*, 41:8512–8518.

Deguillaume, L., Leriche, M., Desboeufs, K., Mailhot, G., George, C., and Chaumerliac, N. (2005). Transition Metals in Atmospheric Liquid Phases: Sources, Reactivity, and Sensitive Parameters. *Chem. Rev.*, 105:3388–3431. <Go to ISI>://000231916100008.

Dellinger, B., Pryor, W. A., Cueto, R., Squadrito, G. L., Hegde, V., and Deutsch, W. A. (2001). Role of Free Radicals in the Toxicity of Airborne Fine Particulate Matter. *Chem. Res. Toxicol.*, 14:1371–1377.

Diaz, E. A., Chung, Y., Lamoureux, D. P., Papapostolou, V., Lawrence, J., Long, M. S., Mazzaro, V., Buonfiglio, H., Sato, R., Koutrakis, P., and Godleski, J. J. (2013). Effects of Fresh and Aged Traffic-Related Particles on Breathing Pattern, Cellular Responses, and Oxidative Stress. *Air Qual. Atmos. Health*, 6:431–444. DOI: 10.1007/s11869-012-0179-2.

DiStefano, E., Eiguren-Fernandez, A., Delfino, R. J., Sioutas, C., Froines, J. R., and Cho, A. K. (2009). Determination of Metal-Based Hydroxyl Radical Generating Capacity of Ambient and Diesel Exhaust Particles. *Inhal. Toxicol..*, 21:731–738.

Donahue, N. M., Henry, K. M., Mentel, T. F., Kiendler-Scharr, A., Spindler, C., Bohn, B., Brauers, T., Dorn, H. P., Fuchs, H., and Tillmann, R. (2012). Aging of Biogenic Secondary Organic Aerosol Via Gas-Phase OH Radical Reactions. *Proc. Natl. Acad. Sci.*, 109:13503–13508.

Engelhart, G., Asa-Awuku, A., Nenes, A., and Pandis, S. (2008). CCN Activity and Droplet Growth Kinetics of Fresh and Aged Monoterpene Secondary Organic Aerosol. *Atmos. Chem. Phys.*, 8:3937–3949.

Fang, T., Verma, V., Guo, H., King, L. E., Edgerton, E. S., and Weber, R. J. (2014). A Semi-Automated System for Quantifying the Oxidative Potential of Ambient Particles in Aqueous Extracts Using the Dithiothreitol (DTT) Assay: Results from the Southeastern Center for Air Pollution and Epidemiology (SCAPE). *Atmos. Meas. Tech. Discuss.*, 7:7245–7279.

Godri, K. J., Harrison, R. M., Evans, T., Baker, T., Dunster, C., Mudway, I. S., and Kelly, F. J. (2011). Increased Oxidative Burden Associated with Traffic Component of Ambient Particulate Matter at Roadside and Urban Background Schools Sites in London. *PLoS One*, 6:e21961. DOI: 10.1371/journal.pone.0021961.

Gonzalez, D. H., Cala, C. K., and Paulson, S. E. HULIS Enhancement of OH by Fe(II): Kinetics of Suwannee RIver Fulvic Acid-Fe(II) Complexes in the Presence of Lung Antioxidants. *Environ. Sci. Technol.*, (submitted).

Graedel, T., Mandich, M., and Weschler, C. (1986). Kinetic Model Studies of Atmospheric Droplet Chemistry: 2. Homogeneous Transition Metal Chemistry in Raindrops. *J. Geophys. Res.: Atmos.*, 91:5205–5221.

Hansen, A., Rosen, H., and Novakov, T. (1984). The Aethalometer—An Instrument for the Real-Time Measurement of Optical Absorption by Aerosol Particles. *Sci. Total Environ.*, 36:191–196.

Heikkilä, J., Happonen, M., Murtonen, T., Lehto, K., Sarjovaara, T., Larmi, M., Keskinen, J., and Virtanen, A. (2012). Study of Miller Timing on Exhaust Emissions of a Hydrotreated Vegetable Oil (HVO)-Fueled Diesel Engine. *J. Air Waste Manage. Assoc.* 62:1305–1312.

ICCT, T I C O C T. (2014). The End of the Era of Heavy Fuel Oil in Maritime Shipping. Available at http://www.theicct.org/blogs/staff/end-era-heavy-fuel-oil-maritime-shipping

Jalava, P. I., Aakko-Saksa, P., Murtonen, T., Happo, M. S., Markkanen, A., Yli-Pirilä, P., Hakulinen, P., Hillamo, R., Mäki-Paakkanen, J., and Salonen, R. O. (2012). Toxicological Properties of Emission Particles from Heavy Duty Engines Powered by Conventional and Bio-Based Diesel Fuels and Compressed Natural Gas. *Part. Fibre Toxicol.*, 9:37. DOI: 10.1186/1743-8977-9-37.

Kelly, F., Cotgrove, M., and Mudway, I. (1995). Respiratory Tract Lining Fluid Antioxidants: the First Line of Defence Against Gaseous Pollutants. *Central Eur. J. Public Health*, 4:11–14.

Kim, D., Kim, S., Oh, S., and No, S-Y. (2014). Engine Performance and Emission Characteristics of Hydrotreated Vegetable Oil in Light Duty Diesel Engines. *Fuel*, 125:36–43.

King, L. E., and Weber, R. J. (2013). Development and Testing of an Online Method to Measure Ambient Fine Particulate Reactive Oxygen Species (ROS) Based on the 2′,7′-Dichlorofluorescin (DCFH) Assay. *Atmos. Meas. Tech.*, 6:1647–1658. DOI: 10.5194/amt-6-1647-2013.

Larsen, B. R., Di Bella, D., Glasius, M., Winterhalter, R., Jensen, N. R., and Hjorth, J. (2001). Gas-phase OH Oxidation of Monoterpenes: Gaseous and Particulate Products. *J. Atmos. Chem.*, 38:231–276.

Li, N., Hao, M., Phalen, R. F., Hinds, W. C., and Nel, A. E. (2003). Particulate Air Pollutants and Asthma: A Paradigm for the Role of Oxidative Stress in PM-Induced Adverse Health Effects. *Clinic. Immunol.*, 109:250–265.

Li, Q., Wyatt, A., and Kamens, R. M. (2009). Oxidant Generation and Toxicity Enhancement of Aged-Diesel Exhaust. *Atmospheric Environment*, 43(3):1037–1042.

Lin, C.-C., Chen, S.-J., Huang, K.-L., Hwang, W.-I., Chang-Chien, G.-P., and Lin, W.-Y. (2005). Characteristics of Metals in Nano/Ultrafine/Fine/Coarse Particles Collected Beside a Heavily Trafficked Road. *Environ. Sci. Technol.*, 39:8113–8122.

Lund, L. G., and Aust, A. E. (1992). Iron Mobilization from Crocidolite Asbestos Greatly Enhances Crocidolite-Dependent Formation of DNA Single-Strand Breaks in øX174 RFI DNA. *Carcinogenesis*, 13:637–642.

Matthews, R. W. (1980). The Radiation-Chemistry of the Terephthalate Dosimeter. *Radiat. Res.*, 83:27–41. DOI: 10.2307/3575256.

McWhinney, R. D., Badali, K., Liggio, J., Li, S.-M., and Abbatt, J. P. (2013). Filterable Redox Cycling Activity: A Comparison Between Diesel Exhaust Particles and Secondary Organic Aerosol Constituents. *Environmental Science & Technology* 47(7):3362–3369.

Nigam, A. (2007). *Emissions Assessment of Selected Diesel Sources at Ports: Baseline Conditions and Benefits Through use of Control Technologies*. PhD Thesis, University of California at Riverside, Rigerside, CA.

Oeder, S., Kanashova, T., Sippula, O., Sapcariu, S. C., Streibel, T., Arteaga-Salas, J. M., Passig, J., Dilger, M., Paur, H.-R., and Schlager, C. (2015). Particulate Matter from Both Heavy Fuel Oil and Diesel Fuel Shipping Emissions Show Strong Biological Effects on Human Lung Cells at Realistic and Comparable in Vitro Exposure Conditions. *PLoS One*, 10:e0126536.

Paris, R., and Desboeufs, K. (2013). Effect of Atmospheric Organic Complexation on Iron-Bearing Dust Solubility. *Atmos. Chem. Phys.*, 13:4895–4905.

Paulson, S. E., Hasson, A., Anastasio, C., Kuang, X. M., Scott, J. A., Gonzalez, D. H., Charbouillot, T., Vu, K. K.-T., Baroi, J., Olea, C., Lolinco, A., Markarian, K., Charrier, J. G., McFall, A. S., and Richards-Henderson, N. K. (2016). *Probing the Intrinsic Ability of Particles to Generate Reactive Oxygen Species and the Effect of Physiologically Relevant Solutes. California Air Resources Board Annual Report.* Available at https://www.arb.ca.gov/research/apr/past/10-314-1.pdf, https://www.arb.ca.gov/research/apr/past/10-314-2.pdf

Price, D., Chen, C.-L., Lamjiri, M. A., Betha, R., Sanchez, K., Liu, J., Lee, A. K. Y., Cocker, D. R., and Russell, L. M. (2017). More Unsaturated, Cooking-Type Hydrocarbon-Like Organic Aerosol Particle Emissions from Renewable Diesel Compared to Ultra Low Sulfur Diesel in At-Sea Operations of a Research Vessel. *Aerosol Sci. Technol.*, 51(2):135–146.

Prokopowicz, A., Zaciera, M., Sobczak, A., Bielaczyc, P., and Woodburn, J. (2015). The Effects of Neat Biodiesel and Biodiesel and HVO Blends in Diesel Fuel on Exhaust Emissions from a Light Duty Vehicle with a Diesel Engine. *Environ. Sci. Technol.*, 49:7473–7482.

Rattanavaraha, W., Rosen, E., Zhang, H., Li, Q., Pantong, K., and Kamens, R. M. (2011). The Reactive Oxidant Potential of Different Types of Aged Atmospheric Particles: An Outdoor Chamber Study. *Atmos. Environ.*, 45:3848–3855.

Reid, J. S., Eck, T. F., Christopher, S. A., Hobbs, P. V., and Holben, B. (1999). Use of the Ångstrom Exponent to Estimate the Variability of Optical and Physical Properties of Aging Smoke Particles in Brazil. *J. Geophys. Res.: Atmos.*, 104:27473–27489.

Sato, K., Nakao, S., Clark, C. H., Qi, L., and Cocker Iii, D. R. (2011). Secondary Organic Aerosol Formation from the Photooxidation of Isoprene, 1, 3-Butadiene, and 2, 3-Dimethyl-1, 3-Butadiene Under High NO x Conditions. *Atmos. Chem. Phys.*, 11:7301–7317.

Shen, H., Barakat, A. I., and Anastasio, C. (2011). Generation of Hydrogen Peroxide from San Joaquin Valley Particles in a Cell-Free solution. *Atmos. Chem. Phys.*, 11:753–765. DOI: 10.5194/acp-11-753-2011.

Shilling, J. E., King, S. M., Mochida, M., and Martin, S. T. (2007). Mass Spectral Evidence that Small Changes in Composition Caused by Oxidative Aging Processes Alter Aerosol CCN Properties. *J. Phys. Chem. A*, 111:3358–3368. DOI: 10.1021/jp068822r.

Shrivastava, M. K., Lane, T. E., Donahue, N. M., Pandis, S. N., and Robinson, A. L. (2008). Effects of Gas Particle Partitioning and Aging of Primary Emissions on Urban and Regional Organic Aerosol Concentrations. *J. Geophys. Res. Atmos.*, 113:D18301 DOI: 10.1029/2007JD009735.

Smith, K. R., and Aust, A. E. (1997). Mobilization of Iron from Urban Particulates Leads to Generation of Reactive Oxygen Species in vitro and Induction of Ferritin Synthesis in Human Lung Epithelial Cells. *Chem. Res. Toxicol.*, 10:828–834.

Storey, J., Curran, S., Dempsey, A., Lewis, S., Walker, N. R., Reitz, R., and Wright, C. (2015). The Contribution of Lubricant to the Formation of Particulate Matter with Reactivity Controlled Compression Ignition in Light-Duty Diesel Engines. *Emission Control Sci. Technol.*, 1:64–79.

Sun, Y., and Pignatello, J. J. (1992). Chemical Treatment of Pesticide Wastes. Evaluation of Iron (III) Chelates for Catalytic Hydrogen Peroxide Oxidation of 2, 4-D at Circumneutral pH. *J. Agric. Food Chem.*, 40:322–327.

Tan, K. H. (2014). *Humic Matter in Soil and the Environment: Principles and Controversies.* CRC Press, Boca Raton, FL.

Verma, V., Shafer, M. M., Schauer, J. J., and Sioutas, C. (2010). Contribution of Transition Metals in the Reactive Oxygen Species Activity of PM Emissions from Retrofitted Heavy-Duty Vehicles. *Atmos. Environ.*, 44:5165–5173.

Wang, Y., Arellanes, C., and Paulson, S. E. (2012). Hydrogen Peroxide Associated with Ambient Fine Mode, Diesel and Biodiesel Aerosol Particles in Southern California. *Aerosol Sci. Technol.*, 46:394–402.

Wang, Y., Chung, A., and Paulson, S. E. (2010). The Effect of Metal Salts on Quantification of Elemental and Organic Carbon in Diesel Exhaust Particles Using Thermal-Optical Evolved Gas Analysis. *Atmos. Chem. Phys.*, 10:11447–11457. DOI: 10.5194/acp-10-11447-2010.

Wang, Y.-F., Huang, K.-L., Li, C.-T., Mi, H.-H., Luo, J.-H., and Tsai, P.-J. (2003). Emissions of Fuel Metals Content from a Diesel Vehicle Engine. *Atmos. Environ.*, 37:4637–4643.

Weng, L., Temminghoff, E. J., Lofts, S., Tipping, E., and Van Riemsdijk, W. H. (2002). Complexation with Dissolved Organic Matter and Solubility Control of Heavy Metals in a Sandy Soil. *Environ. Sci. Technol.*, 36:4804–4810.

Westphal, G. T. A., Krahl, J. R., Munack, A., Rosenkranz, N., Schröder, O., Schaak, J., Pabst, C., Brüning, T., and Bünger, J. R. (2013). Combustion of Hydrotreated Vegetable Oil and Jatropha Methyl Ester in a Heavy Duty Engine: Emissions and Bacterial Mutagenicity. *Environ. Sci. Technol.*, 47:6038–6046.

Zhang, X., Chen, Z., and Zhao, Y. (2010). Laboratory Simulation for the Aqueous OH-Oxidation of Methyl Vinyl Ketone and Methacrolein: Significance to the in-Cloud SOA Production. *Atmos. Chem. Phys.*, 10:9551–9561.

Zhang, Y., Schauer, J. J., Shafer, M. M., Hannigan, M. P., and Dutton, S. J. (2008). Source Apportionment of in Vitro Reactive Oxygen Species Bioassay Activity from Atmospheric Particulate Matter. *Environ. Sci. Technol.*, 42:7502–7509.